

Grand-canonical Peierls theory for atomic wires on substrates

Yasemin Ergün* and Eric Jeckelmann†

Leibniz Universität Hannover, Institut für Theoretische Physik, Appelstrasse 2, 30167 Hannover, Germany (Received 28 August 2019; revised manuscript received 28 November 2019; accepted 22 January 2020; published 4 February 2020)

We present a generic grand-canonical theory for the Peierls transition in atomic wires deposited on semiconducting substrates such as In/Si(111) using a mean-field solution of the one-dimensional Su-Schrieffer-Heeger model. We show that this simple low-energy effective model for atomic wires can explain naturally the occurrence of a first-order Peierls transition between a uniform metallic phase at high temperature and a dimerized insulating phase at low temperature as well as the existence of a metastable uniform state below the critical temperature.

DOI: [10.1103/PhysRevB.101.085403](https://doi.org/10.1103/PhysRevB.101.085403)**I. INTRODUCTION**

The Peierls instability of a one-dimensional metal coupled to lattice vibrations [1] is a hallmark of low-dimensional physics. It is known to play an important role in various strongly anisotropic bulk materials and there is a well-established theoretical framework to describe these quasi-one-dimensional systems at a fixed electronic density [2–5]. In particular, the canonical Peierls theory predicts a continuous transition from a metallic state with a uniform lattice at high temperature to an insulating state with a distorted lattice at low temperature.

Atomic wires deposited on a semiconducting substrate [6,7] represent another possible realization of one-dimensional electronic systems in which the Peierls instability could play a role. Indeed, the Peierls mechanism was invoked to explain the metal-insulator transition accompanied by a structural transition with a doubling of the unit cell observed in indium wires on a Si(111) surface [8]. Various other explanations have been proposed for this transition, however, and the relevance of the Peierls mechanism remains controversial. The common problem with most previous interpretations of experiments and first-principles simulations is that they do not consider how the semiconducting substrate modifies the predictions of the one-dimensional Peierls theory.

Recent experimental evidence and first-principles simulations for In/Si(111) suggest that the metallic uniform state remains metastable below the critical temperature and that the transition is first order in this system [9–16]. In Ref. [14] it was shown that the first-principles simulation results, the metastability of the metallic uniform state, and the first-order transition could be understood within a grand-canonical Peierls theory based on an effective one-dimensional low-energy model. The indium wires were described by a specifically constructed Hamiltonian of the Su-Schrieffer-Heeger (SSH) type [17,18] including four electronic bands and three commensurate lattice distortion modes while the substrate

was treated as a charge reservoir for the wire subsystem. However, the first-order transition was only obtained under the assumption that the chemical potential must vary with temperature to preserve the overall charge neutrality. Moreover, the model was investigated purely numerically and only for the parameters that were obtained from first-principles simulations of In/Si(111).

In this paper we present a generic grand-canonical Peierls theory based on the original SSH model with one electronic band and one commensurate lattice distortion mode in the mean-field approximation (dimerization). The substrate only acts as an electron reservoir and sets the chemical potential for the wires. Using only analytical results and basic numerical calculations we demonstrate that in a grand-canonical Peierls system the high-temperature uniform metallic state can remain thermodynamically metastable below the critical temperature. Additionally, we show that the structural Peierls phase transition can be first order as a function of temperature for a fixed chemical potential. Moreover, we find that the metal-insulator transition is always first order.

In the next section we introduce the grand-canonical mean-field approach for atomic wires on semiconducting substrates based on the SSH model. In Sec. III we recapitulate the known results for the Peierls transition in the SSH model at half-filling. Our results for the SSH model in the grand-canonical ensemble are presented in Sec. IV. Finally, Sec. V contains our conclusions. Some details are presented in two Appendixes.

II. GRAND-CANONICAL MODEL FOR THE PEIERLS TRANSITION**A. SSH model**

The SSH model [3,4,17,18] is the standard model for charge density waves (CDW) on bonds caused by a Peierls distortion of bond lengths. It consists of a one-dimensional lattice with L sites (ions) and $N/2$ electrons of each spin. The lattice degrees of freedom are treated classically. The position of site j along the lattice axis is given by $x_j = ja + u_j$, where a is the lattice constant of the uniform lattice configuration

*yasemin.erguen@itp.uni-hannover.de

†eric.jeckelmann@itp.uni-hannover.de

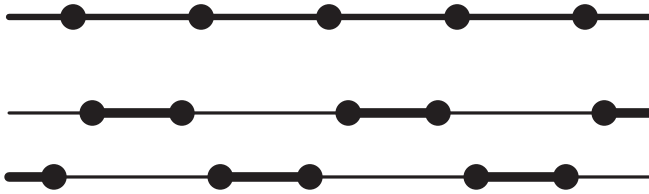


FIG. 1. Schematic of the uniform lattice configuration (top) and the two dimerized configurations (bottom) in the SSH model. The disks represent the sites (atoms) and the linewidths show the strength of the bond order or hopping term.

($x_j = ja$) shown in Fig. 1, while u_j describes the deviation from this position. The Hamilton function for the lattice degrees of freedom (without coupling to the electrons) is

$$\mathcal{H} = \sum_j \frac{P_j^2}{2M} + V, \quad (1)$$

where P_j designates the conjugate momentum of u_j , M is the effective mass of the ions, and V is the lattice elastic energy. For small deviations u_j the lattice elastic energy can be approximated by a harmonic potential

$$V = \frac{K}{2} \sum_j (u_{j+1} - u_j)^2, \quad (2)$$

with the spring constant K . We will use periodic boundary conditions $u_{L+1} \equiv u_1$ and thus sums over the site index j always runs from 1 to L .

A tight-binding Hamiltonian is used for the electronic degrees of freedom and it is assumed that the only relevant hopping terms are between nearest-neighbor sites (including the coupling to the lattice deformations). The Hamilton operator is

$$H = - \sum_{j,\sigma} t_j (c_{j,\sigma}^\dagger c_{j+1,\sigma} + c_{j+1,\sigma}^\dagger c_{j,\sigma}), \quad (3)$$

where the operator $c_{j,\sigma}^\dagger$ ($c_{j,\sigma}$) creates (annihilates) an electron with spin σ ($=\uparrow, \downarrow$) on site j . The hopping term t_j depends on the distance between the sites j and $j+1$, i.e., $t_j = t(u_{j+1} - u_j)$. In the SSH approach a linear dependence is assumed for small deviations u_j ,

$$t_j = t_0 - \alpha(u_{j+1} - u_j), \quad (4)$$

with the electron-phonon coupling constant $\alpha \geq 0$ and the value t_0 of the hopping for the uniform lattice configuration. As the sign of the hopping terms can be changed with a simple gauge transformation $c_{j\sigma}^\dagger \rightarrow (-1)^j c_{j\sigma}^\dagger$, it is sufficient to consider the case $t_j > 0$ ($\Rightarrow t_0 > 0$).

Note that this linear approximation for $t(u_{j+1} - u_j)$ is inconsistent with the quadratic approximation for the lattice potential (2). As this inconsistency does not change the results qualitatively, we will keep to the SSH choice in this paper. See Appendix A for more details.

B. Dimerization

In this work we will exclusively consider the mean-field approximation for a commensurate Peierls distortion of period

two (dimerization) and thus assume that

$$u_j = (-1)^j u, \quad (5)$$

with a constant alternating site displacement u [3,4,17,18]. This corresponds to alternating long and short bonds, as shown in Fig. 1. This particular lattice distortion is the normal mode of the classical oscillator system (1) with wave number $Q = \pi/a$ and thus the unstable $2k_F$ mode of the Peierls theory at half-filling [$k_F = \pi/(2a) \Rightarrow Q = \pi/a$]. The displacement amplitude u is related to the usual Peierls order parameter (or dimerization parameter) by

$$\Delta = 4\alpha u. \quad (6)$$

It will be convenient to work with the dimensionless order parameter

$$\delta = \frac{\Delta}{2t_0} = \frac{2\alpha u}{t_0}. \quad (7)$$

The lattice elastic energy (2) becomes

$$V = \frac{Lt_0}{\pi\lambda} \delta^2, \quad (8)$$

with the dimensionless SSH electron-phonon coupling

$$\lambda = \frac{2\alpha^2}{\pi K t_0}. \quad (9)$$

In Ref. [14] it was shown that $\lambda = 0.37$ and 0.18 were realistic values for the shear and rotary Peierls modes of indium wires on Si(111), respectively. The lattice kinetic energy can also be written as a function of the order parameter

$$E_K = \frac{Lt_0}{\pi\lambda} \frac{\delta^2}{\omega_0^2}, \quad (10)$$

where $\dot{\delta}$ designates the time derivative of the order parameter δ and

$$\omega_0 = \sqrt{\frac{4K}{M}} \quad (11)$$

is the bare frequency of amplitude fluctuations of the order parameter (i.e., the normal mode with wave number $Q = \pi/a$) when the lattice is not coupled to the electrons.

From assumption (5) follows that the hopping terms t_j alternate between two values and thus we can compute the single-particle eigenstates of the electronic Hamiltonian (3) exactly. The single-electron eigenenergies are given by

$$\varepsilon_s(k) = s2t_0 \sqrt{\cos^2(ka) + \delta^2 \sin^2(ka)}, \quad (12)$$

with the band index $s = \pm 1$ and the wave number $k = 2\pi z/(La)$ for integers $-L/4 < z \leq L/4$, which implies $k \in (-\pi/(2a), \pi/(2a)]$. We see in Fig. 2 that the spectrum contains a gap of width

$$E_g = 2|\Delta| = 4t_0|\delta| \quad (13)$$

centered around the energy $\varepsilon = 0$. Consequently, δ (or Δ) is also called gap parameter. At half-filling (and more generally for a chemical potential $|\mu| < |\Delta| = 2t_0|\delta|$) the electronic system is an insulator for $\delta \neq 0$ while it is metallic for $\delta = 0$. The assumption of small position deviations $|u_j| = |u|$ used above can now be formulated quantitatively as the condition $|\delta| < 1$.

A vanishing order parameter $\delta = 0$ corresponds to a uniform lattice structure and a constant density while a finite

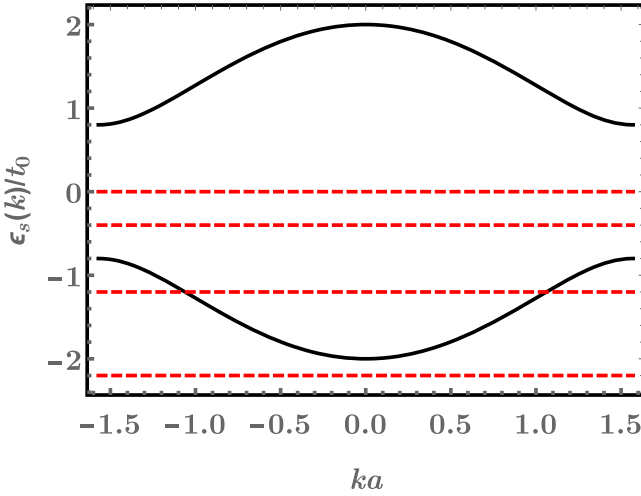


FIG. 2. Dispersion (12) of the single-electron eigenenergies for $\Delta = 2\delta t_0 = 0.8t_0$. The horizontal dashed lines show the four different relative positions of the chemical potential: $\mu = 0$ (half-filling), $0 > \mu > -\Delta$, $-\Delta > \mu > -2t_0$, and $-2t_0 > \mu$ (see the discussion in Sec. IV A).

order parameter $\delta \neq 0$ corresponds to a dimerized lattice and a CDW on the bonds. Moreover, in the canonical ensemble at half-filling, the uniform configuration yields a metallic state while the dimerized one corresponds to an insulator as discussed above. As the SSH model in the mean-field approximation (5) is invariant under simultaneous reflection ($u \rightarrow -u$) and translation ($j \rightarrow j + 1$) transformations, configurations with opposite order parameters (δ and $-\delta$) have the same energy. Consequently, the ground state is doubly degenerate in the dimerized phase, as illustrated in Fig. 1.

C. Grand-canonical potential

Our goal is to determine the equilibrium properties of the SSH model at finite temperature T . For wire-substrate systems such as In/Si(111), the number of electrons N is not fixed but the chemical potential μ is set by the substrate, which acts as a reservoir [14]. Thus we will use the grand-canonical ensemble for the electronic degrees of freedom but the canonical ensemble for the lattice degrees of freedom because we assume that the number of sites (atoms) in the chain is fixed.

After tracing out the electronic degrees of freedom we obtain the grand-canonical potential of the full system per lattice site

$$\phi = \frac{t_0}{\pi\lambda} \delta^2 - \frac{k_B T}{L} \sum_{k,s,\sigma} \ln(1 + \exp\{-\beta[\varepsilon_s(k) - \mu]\}), \quad (14)$$

with $1/\beta = k_B T$. In the thermodynamic limit $L \rightarrow \infty$ one can write

$$\phi = \frac{t_0}{\pi\lambda} \delta^2 - \mu - k_B T \ln(2) - k_B T \int_{|\Delta|}^{2t_0} d\varepsilon D(\varepsilon) \ln [\cosh(\beta\mu) + \cosh(\beta\varepsilon)], \quad (15)$$

where the single-particle density of states is given by

$$D(\varepsilon) = \frac{2}{\pi} \frac{|\varepsilon|}{\sqrt{(4t_0^2 - \varepsilon^2)(\varepsilon^2 - \Delta^2)}} \quad (16)$$

for $\Delta < |\varepsilon| < 2t_0$. Using a substitution $z = \varepsilon/(2t_0)$ one can easily verify that ϕ depends only on the two thermodynamical variables T and μ , the two model parameters λ and t_0 (the latter just sets the energy scale), and the order parameter δ . We also note that ϕ is an even function of δ .

Within this mean-field, semiclassical approach the grand-canonical potential (15) plays the role of the Landau's free energy for the order parameter δ of the commensurate Peierls transition [2]. The actual grand-canonical potential $\phi(T, \mu)$ and the stable configurations $\delta(T, \mu)$ are given by the minima of (15) with respect to variations of δ . Thus our main goal is to determine the stable configurations and the related observables as a function of T and μ , as well as the single remaining model parameter λ .

In the grand-canonical ensemble the average electronic density for a given temperature T and chemical potential μ is given by

$$\rho = \frac{N}{L} = \frac{1}{L} \sum_{k,s,\sigma} f[\varepsilon_s(k)], \quad (17)$$

with the Fermi-Dirac distribution

$$f(\varepsilon) = \frac{1}{1 + \exp[\beta(\varepsilon - \mu)]}. \quad (18)$$

In the thermodynamic limit we can write

$$\rho = 1 + \int_{|\Delta|}^{2t_0} d\varepsilon D(\varepsilon) \frac{\sinh(\beta\mu)}{\cosh(\beta\mu) + \cosh(\beta\varepsilon)}. \quad (19)$$

We see that for $\mu = 0$ the electronic band is half-filled ($\rho = 1$) while less than half-filling ($0 \leq \rho < 1$) corresponds to $\mu < 0$ and more than half-filling ($1 < \rho \leq 2$) to $\mu > 0$. Because the SSH model is invariant under the particle-hole transformation $c_{j\sigma}^\dagger \rightarrow (-1)^j c_{j\sigma}$, the results are similar for $\mu \leq 0$ and $\mu \geq 0$, and thus we will discuss the first case only.

Equations (15) and (19) are the starting point for studying thermodynamical Peierls transitions in the SSH model at the mean-field level. Usually it is assumed that the electronic density is fixed and the grand-canonical ensemble is used only for computational convenience [2,5]. Therefore, the value of the chemical potential is set by Eq. (19) for the desired value of ρ . In Sec. III we will summarize the results obtained with this assumption for the Peierls transition at half-filling. In Sec. IV we will then generalize these results for a fixed chemical potential.

III. RESULTS AT FIXED BAND FILLING

The conventional Peierls theory assumes a fixed electronic density ρ . For the dimerized SSH model the band is usually half-filled ($\rho = 1$) which corresponds to $\mu = 0$ according to (19). Here we summarize the most important results for this case [2–5,17–19]. The grand-canonical potential (15) is then

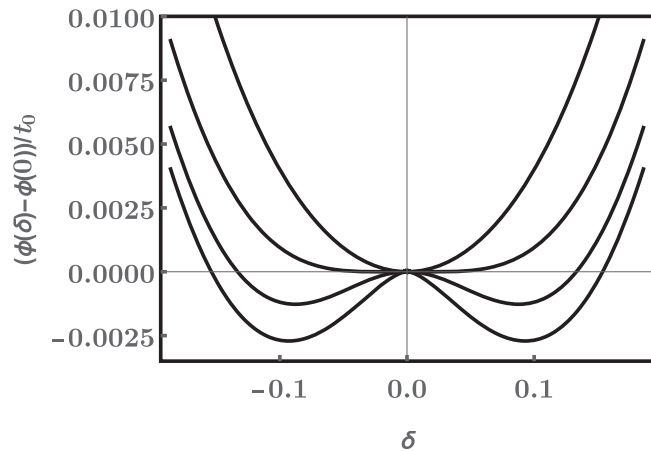


FIG. 3. Grand-canonical potential (15) at $\mu = 0$ (half-filling) [see Eq. (20)] as a function of the order parameter δ for $\lambda = 0.18$ and four different temperatures (from bottom to top): $T \approx 0$, $T \approx T_p/2$, $T \approx T_p$, and $T \approx 2T_p$.

simplified

$$\phi = \frac{t_0}{\pi\lambda} \delta^2 - k_B T \ln(2) - k_B T \int_{|\Delta|}^{2t_0} d\varepsilon D(\varepsilon) \ln [1 + \cosh(\beta\varepsilon)]. \quad (20)$$

For high temperatures ($k_B T \gg t_0$) it can be approximated by

$$\phi = \frac{t_0}{\pi\lambda} \delta^2 - k_B T \ln(4). \quad (21)$$

Therefore the uniform metallic configuration ($\delta = 0$) is the only stable phase at high temperatures.

For low temperatures ($T \rightarrow 0$) the grand-canonical potential (20) yields the ground-state energy

$$\begin{aligned} \phi &= \frac{t_0}{\pi\lambda} \delta^2 - \int_{|\Delta|}^{2t_0} d\varepsilon D(\varepsilon) \varepsilon \\ &= \frac{t_0}{\pi\lambda} \delta^2 - \frac{4t_0}{\pi} E(1 - \delta^2), \end{aligned} \quad (22)$$

where $E(m)$ is the complete elliptic integral of the second kind. It is well known that this expression is a double-well potential as a function of δ ($|\delta| < 1$) with two minima at $\delta = \pm\delta_0 \neq 0$ and a local maximum at $\delta = 0$, see the lower curve in Fig. 3. Throughout this paper we denote with $\delta_0 = \Delta_0/(2t_0) = \delta(T = 0, \mu = 0)$ the absolute value of the order parameter for the stable configuration at half-filling and zero temperature.

For small δ we can expand (22) up to the lowest relevant order in δ ,

$$\phi = \frac{t_0}{\pi\lambda} \delta^2 - \frac{4t_0}{\pi} \left\{ 1 + \frac{1}{2} \left[\ln \left(\frac{4}{|\delta|} \right) - \frac{1}{2} \right] \delta^2 \right\}. \quad (23)$$

Then one can easily verify that ϕ has a double minimum for $\delta = \pm\delta_0$ with

$$\delta_0 = \frac{4}{e} \exp \left(-\frac{1}{2\lambda} \right). \quad (24)$$

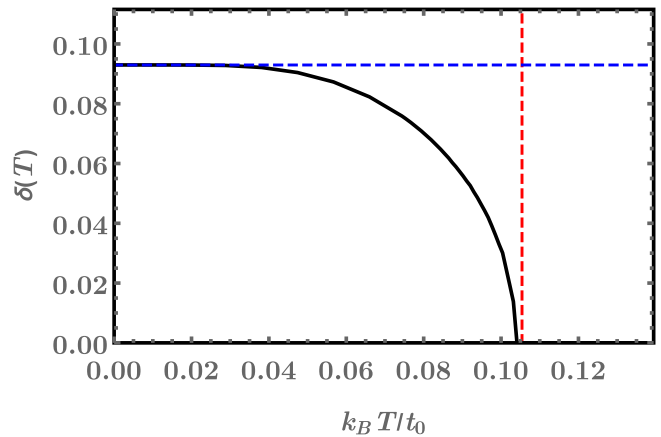


FIG. 4. Order parameter δ as a function of temperature at half-filling for the electron-phonon coupling $\lambda = 0.18$. The horizontal line shows the zero-temperature value δ_0 obtained from the minimization of the ground-state energy (22) while the vertical line shows the critical temperature (31).

We see that this calculation is valid for weak electron-phonon coupling because $\delta_0 \ll 1 \Leftrightarrow \lambda \ll 1$. As an example, for $\lambda = 0.18$ we obtain $\delta_0 \approx 0.0915$ from (24) and $\delta_0 \approx 0.0930$ from the numerical minimization of the energy (22). The condensation energy of the dimerized state per site [i.e., the difference between the ground-state energy (23) at $\delta = 0$ and at its minimum] is

$$\Delta\phi = \frac{t_0}{\pi} \delta_0^2. \quad (25)$$

The Peierls theory predicts the existence of Raman-active collective excitations (electronic CDW and lattice vibrations), which correspond to amplitude oscillations of the order parameter δ around its equilibrium configuration in the mean-field approach [2,20–22]. The effective spring constant for these oscillations is given by the second derivative of ϕ with respect to δ at its minimum. Combined with the kinetic energy (10) this leads to the renormalized (phonon) frequency for amplitude fluctuations

$$\Omega^2 = \frac{\pi\lambda}{2t_0} \frac{d^2\phi}{d\delta^2} \omega_0^2, \quad (26)$$

where ω_0 is the frequency (11) of the bare phonon mode with wave number $Q = 2k_F$. For the weak-coupling regime ($\lambda \ll 1$) we obtain using (23) and (24) [3,4,23]

$$\Omega^2 = 2\lambda\omega_0^2. \quad (27)$$

As the grand-canonical potential (20) has one minimum at $\delta = 0$ for high temperatures and two minima at $\pm\delta \neq 0$ at zero temperature, there is a phase transition at a (mean-field) critical temperature T_p . One can easily determine numerically the value of the order parameter that minimizes (20) for a given temperature T . The result for $\lambda = 0.18$ is shown in Fig 4. Clearly there is a continuous transition from the high-temperature uniform metallic phase to the low-temperature dimerized insulating phase at a finite critical temperature $k_B T_p \approx 0.104t_0$.

Figure 5 shows that the renormalized phonon frequency (26) calculated numerically from the second derivative

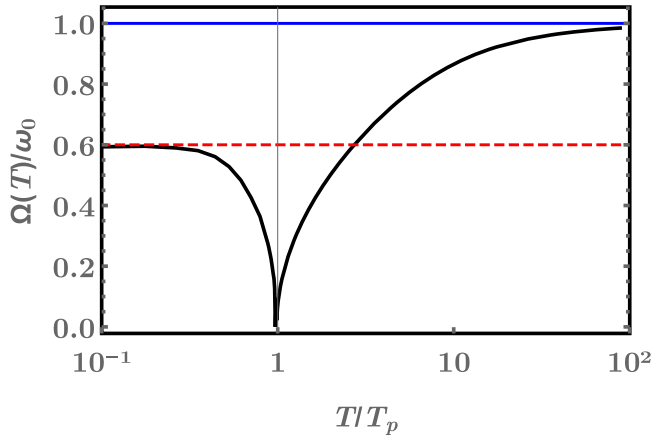


FIG. 5. Renormalized phonon frequency Ω/ω_0 for the amplitude mode [see Eq. (26)] as a function of temperature at half-filling with an electron-phonon coupling $\lambda = 0.18$. The horizontal dashed and solid lines show the zero-temperature frequency (27) and bare phonon frequency, respectively. The vertical line shows the critical temperature T_p , see Eq. (31).

of (20) at its minimum. We see that the phonon mode becomes completely soft at the critical temperature already found for the order parameter in Fig. 4. This vanishing of the amplitude mode frequency is the signature of the Kohn anomaly in the phonon spectrum around the wave number $Q = 2k_F$ [2–5, 20–22] in a mean-field description of the Peierls transition.

From the necessary condition for a minimum

$$\frac{d\phi}{d\delta} = 0 \quad (28)$$

one can deduce the self-consistency equation for solutions $\delta \neq 0$,

$$\frac{1 - \delta^2}{2\lambda} 2t_0 = \int_{|\Delta|}^{2t_0} d\varepsilon \sqrt{\frac{4t_0^2 - \varepsilon^2}{\varepsilon^2 - \Delta^2}} \frac{\sinh(\beta\varepsilon)}{1 + \cosh(\beta\varepsilon)}. \quad (29)$$

If we approximate the spectrum (12) by linear dispersions for $|\varepsilon| \gg |\Delta|$ and treat $2t_0$ as the ultraviolet cutoff, we can approximate $\sqrt{4t_0^2 - \varepsilon^2} \approx 2t_0$ in the above integral. In the weak-coupling regime ($\lambda \ll 1 \Rightarrow \delta_0 \ll 1$) we can then solve the self-consistency equation for $T = 0$ and for $\delta \rightarrow 0$ ($\Leftrightarrow T \rightarrow T_p$). In the ground state ($T = 0$) we obtain

$$\delta'_0 = 2 \exp\left(-\frac{1}{2\lambda}\right), \quad (30)$$

which deviates from the correct result (24) only by a constant factor $e/2$. This factor [like the one due to the SSH hopping term (4), see Appendix A] is only a minor problem because of the one-to-one correspondence between δ_0 , δ'_0 and the single relevant model parameter λ . Thus one can deduce relations between observables and δ'_0 using the above approximation and then substitute the correct value δ_0 to obtain a quantitatively accurate result. This is especially well illustrated by the following determination of the critical temperature.

At the critical temperature one can insert $\delta = 0$ in the self-consistency equation and thus find

$$k_B T'_p = \frac{2t_0 e^\gamma}{\pi} \delta'_0 \approx 1.134 \delta'_0 t_0, \quad (31)$$

with the Euler constant $\gamma \approx 0.577$. This leads to the well-known relation between the (mean-field) critical temperature and the zero-temperature electronic gap (13) [2]

$$k_B T'_c = \frac{e^\gamma}{2\pi} E'_g \approx \frac{E'_g}{3.53}. \quad (32)$$

We see in Figs. 4 and 5 that the relation (31) yields an excellent approximation of the critical temperature for an electron-phonon coupling as large as $\lambda = 0.18$. However, we have to substitute the correct value the zero-temperature order parameter (24), in lieu of the approximate value (30), in the relation (31) to obtain this quantitative agreement. For stronger couplings deviations become significant. For instance, for $\lambda = 0.37$ we obtain $\delta_0 \approx 0.446$ which corresponds to $k_B T_p \approx 0.505 t_0$ according to (31) but we find numerically that $k_B T_p \approx 0.455 t_0$.

IV. RESULTS FOR FIXED CHEMICAL POTENTIAL

We now turn to the general case of a fixed chemical potential $\mu < 0$. (As mentioned earlier the case $\mu > 0$ yields similar results.) For high temperatures ($k_B T \gg t_0$) the grand-canonical potential (15) can be approximated by

$$\phi = \frac{t_0}{\pi\lambda} \delta^2 - \mu - k_B T \ln[2 + 2 \cosh(\beta\mu)]. \quad (33)$$

Therefore, the uniform metallic configuration ($\delta = 0$) is the only stable phase at high temperatures for any value of μ .

A. Ground-state results

The ground-state results (i.e., for $T \rightarrow 0$) are more interesting. The grand-canonical potential (14) yields in the thermodynamic limit

$$\phi = \frac{t_0}{\pi\lambda} \delta^2 - \mu \rho - \frac{4t_0}{\pi} E\left(\frac{\pi}{2} \rho, 1 - \delta^2\right), \quad (34)$$

where $E(\phi, m)$ is the incomplete elliptic integral of the second kind. The electronic density is $\rho = 1$ when the chemical potential lies in the Peierls gap ($0 \geq \mu \geq -|\Delta|$),

$$\rho = \frac{2}{\pi} \arcsin\left(\sqrt{\frac{4t_0^2 - \mu^2}{4t_0^2 - \Delta^2}}\right) \in (0, 1) \quad (35)$$

when it is within the valence band ($-|\Delta| > \mu > -2t_0$), and $\rho = 0$ when it lies below the valence band ($\mu \leq -2t_0$). These three different relative values of the chemical potential μ are illustrated in Fig. 2.

We can now examine the zero-temperature phases as a function of the chemical potential. We note that Eq. (34) for $\mu \geq -|\Delta|$ is equal to the ground-state energy at half-filling (22) up to a constant shift $-\mu$. Consequently, ϕ varies with δ as at half-filling as long as the chemical potential lies in the electronic band gap. Thus we know that for $\mu > -\Delta_0 = -2\delta_0 t_0$ there are two (possibly local) minima at $\delta = \pm\delta_0$ (as at half-filling) and no other extrema for larger values of $|\delta|$.

Similarly to the half-filling case (25) the minima are given at weak coupling by

$$\phi_{\min} = -\frac{4t_0}{\pi} - \mu - \frac{t_0}{\pi} \delta^2. \quad (36)$$

Additionally, we can conclude that there is no extremum for $-\Delta_0 < \mu < -\Delta_0$.

For $\mu < -\Delta_0$ but $|\mu| \ll 2t_0$ we can expand Eq. (34) up to the second order in δ . Using the weak-coupling result for half-filling (24) we find

$$\phi = -\frac{4t_0}{\pi} - \mu - \frac{\mu^2}{2\pi t_0} + \frac{2t_0}{\pi} \ln\left(\frac{2|\mu|}{\Delta_0}\right) \delta^2. \quad (37)$$

For $\mu > -\Delta_0/2$ the coefficient of the quadratic term is negative and thus there is a local maximum at $\delta = 0$ as for half-filling. For $\mu < -\Delta_0/2$, however, the coefficient of δ^2 is positive. Thus there is a (possibly local) minimum at $\delta = 0$. Comparing the energies (36) of the minima at $\delta = \pm\delta_0$ and (37) for the minimum at $\delta = 0$ we see that the dimerized configuration has a lower energy for $\mu > -\sqrt{2}\delta_0 t_0 = -\Delta_0/\sqrt{2}$ while the uniform configuration becomes stable when μ drops below this value.

From the necessary condition (28) one can deduce a self-consistency equation for the extrema of (34) at finite δ . Assuming again a linear electronic dispersion with a cutoff $2t_0$ for $|\varepsilon| \gg |\Delta|$, we obtain solutions that agree with the above analysis of the potential (34). Moreover, the absence of any solution of the self-consistency equation for $\mu < -\Delta_0$ shows that the dimerized state is unstable in this regime. See Appendix B for more details.

In summary, the weak-coupling analysis reveals the existence of four phases at zero temperature. In the first phase for $0 \geq \mu > -\Delta_0/2$, which includes the half-filled band case, the dimerized configuration is stable and the uniform configuration is unstable. In the second phase $-\Delta_0/2 > \mu > -\Delta_0/\sqrt{2}$ the dimerized configuration is still stable but the uniform configuration is now metastable. In the third phase for $-\Delta_0/\sqrt{2} > \mu > -\Delta_0$ the dimerized configuration becomes metastable while the uniform configuration is stable. Finally, in the fourth phase for $-\Delta_0 > \mu$ the uniform configuration is still stable and the dimerized configuration is unstable. Moreover, the order parameter of the (stable or metastable) dimerized configuration has the same value (24) as the one found at half-filling down to $\mu = -\Delta_0$. Thus the value of the zero-temperature order parameter as a function of the chemical potential ($\mu \leq 0$) is

$$\delta(T=0, \mu) = \begin{cases} \pm\delta_0 & \text{for } \mu > -\Delta_0/\sqrt{2}, \\ 0 & \text{for } \mu < -\Delta_0/\sqrt{2}. \end{cases} \quad (38)$$

The potential (34) can easily be calculated numerically as a function of δ for a given chemical potential. The results are shown in Figs. 6–8 for the finite electron-phonon coupling $\lambda = 0.18$. Figure 6 shows that for $\mu = -\Delta_0/4$ the shape of ϕ still resembles the double-well potential shown in Fig. 3 for half-filling. We see clearly that the minima corresponding to the dimerized configuration are progressively raised (relative to the potential of the uniform configuration $\delta = 0$) as μ is lowered until they become metastable (see the curve for

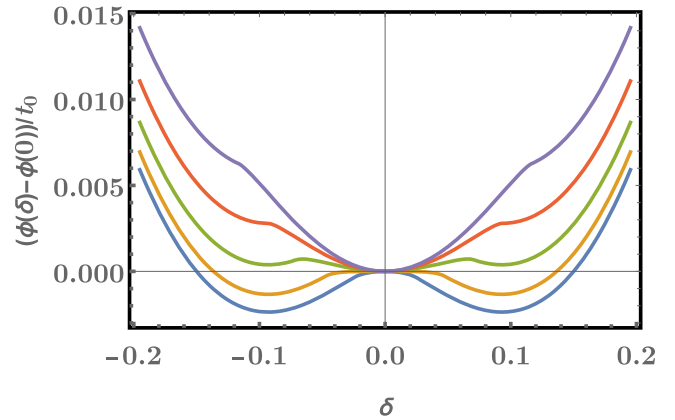


FIG. 6. Grand-canonical potential (15) at zero temperature [see Eq. (34)] as a function of the order parameter δ for $\lambda = 0.18$ and several values of the chemical potential from $\mu = -0.25\Delta_0$ (bottom curve) to $\mu = -1.25\Delta_0$ (top curve) in steps of $-0.25\Delta_0$.

$\mu = -0.75\Delta_0$), and are finally suppressed (see the curve for $\mu = -1.25\Delta_0$).

Figure 7 shows the behavior of ϕ around $\delta = 0$ in more details. We clearly see that the local maximum at $\delta = 0$ becomes a minimum when the chemical potential decreases from $-0.49\Delta_0$ to $-0.495\Delta_0$. The small deviation from the weak-coupling boundary value $-\Delta_0/2$ is due to the finite value of λ . The deviation grows larger with λ , for instance the boundary value reaches $\mu = -0.43\Delta_0$ for $\lambda = 0.37$.

Finally, the existence of metastable states is illustrated in Fig. 8. Clearly we observe an absolute minimum of ϕ at finite δ and a local minimum at $\delta = 0$ for $\mu = -0.625\Delta_0$ while for $\mu = -0.750\Delta_0$ there is an absolute minimum at $\delta = 0$ and a local minimum at finite δ . This agrees with the weak-coupling critical value $\mu = -\Delta_0/\sqrt{2} \approx -0.71\Delta_0$ for the boundary between dimerized and uniform phases. Moreover, we see in Fig. 8 that the order parameter of the (stable or metastable) dimerized state (i.e., the position of the minimum with $\delta \neq 0$)

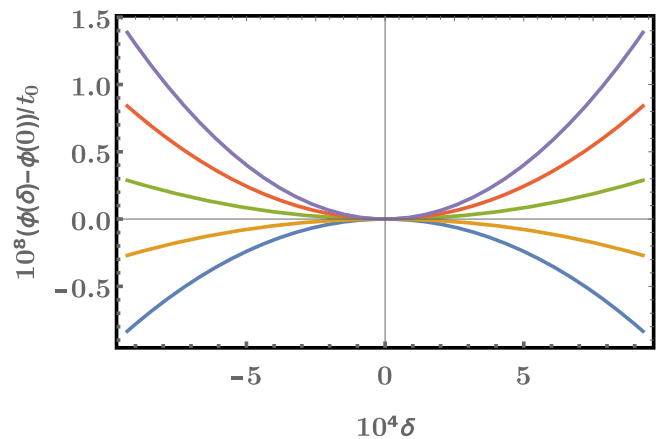


FIG. 7. Grand-canonical potential (15) at zero temperature [see Eq. (34)] as a function of the order parameter δ around $\delta = 0$ for $\lambda = 0.18$ and several values of the chemical potential from $\mu = -0.485\Delta_0$ (bottom curve) to $\mu = -0.505\Delta_0$ (top curve) in steps of $-0.005\Delta_0$.

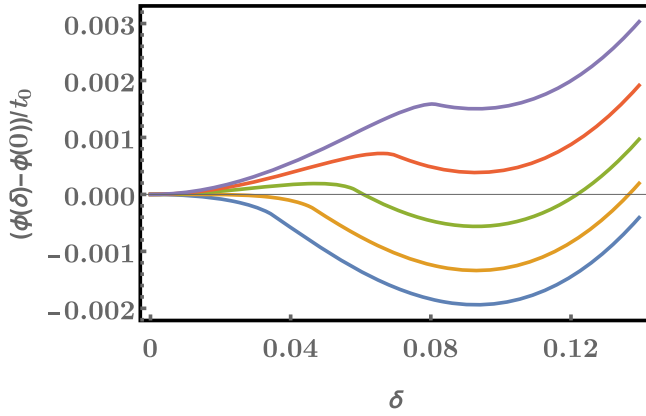


FIG. 8. Grand-canonical potential (15) at zero temperature [see Eq. (34)] as a function of the order parameter $\delta \geq 0$ for $\lambda = 0.18$ and several values of the chemical potential from $\mu = -0.375\Delta_0$ (bottom curve) to $\mu = -0.875\Delta_0$ (top curve) in steps of $-0.125\Delta_0$.

does not vary with μ in agreement with the weak-coupling prediction.

Therefore, the numerical results for the finite electron-phonon coupling $\lambda = 0.18$ in Figs. 6–8 confirm the weak-coupling analysis. In particular, we have found a dimerized phase with a metastable uniform state for $-\Delta_0/2 > \mu > -\Delta_0/\sqrt{2}$ at zero temperature.

B. Finite-temperature phase diagram

We now turn our attention to the still unexplored case $T > 0$ and $\mu < 0$. From the necessary condition for extrema (28) one can deduce the self-consistency equation for the minima and maxima of the grand-canonical potential (15) at finite δ ,

$$\frac{1 - \delta^2}{2\lambda} 2t_0 = \int_{|\Delta|}^{2t_0} d\varepsilon \sqrt{\frac{4t_0^2 - \varepsilon^2}{\varepsilon^2 - \Delta^2}} \frac{\sinh(\beta\varepsilon)}{\cosh(\beta\mu) + \cosh(\beta\varepsilon)}. \quad (39)$$

The solutions $\delta(T, \mu)$ can be easily computed numerically but it is difficult to determine the phase boundary of a continuous transition. However, if $\delta(T, \mu)$ vanishes continuously, the critical values of T and μ must satisfy the self-consistency equation

$$\frac{2t_0}{2\lambda} = \int_0^{2t_0} d\varepsilon \frac{\sqrt{4t_0^2 - \varepsilon^2}}{\varepsilon} \frac{\sinh(\beta\varepsilon)}{\cosh(\beta\mu) + \cosh(\beta\varepsilon)}. \quad (40)$$

The (T, μ) phase diagram for the SSH model in the mean-field approximation can be determined numerically using these two equations. The result is shown in Fig. 9 for the electron-phonon coupling $\lambda = 0.37$ [corresponding to $\delta_0 = 0.446$, $\Delta_0 = 0.891t_0$, and $k_B T_P(\mu = 0) \approx 0.455t_0$]. Results are qualitatively similar for weaker λ . We see that the grand-canonical phase diagram is much richer than for the Peierls transition at fixed band filling (for instance, for $\mu = 0$). It consists of two main phases, the dimerized phase (noted D or D') and the uniform phase (labeled U or U'). We denote $T_P(\mu)$, or equivalently $\mu_P(T)$, the boundary line between these two phases. Each phase is made of two sectors. In the main sectors (D or U) only one state (dimerized or uniform) is

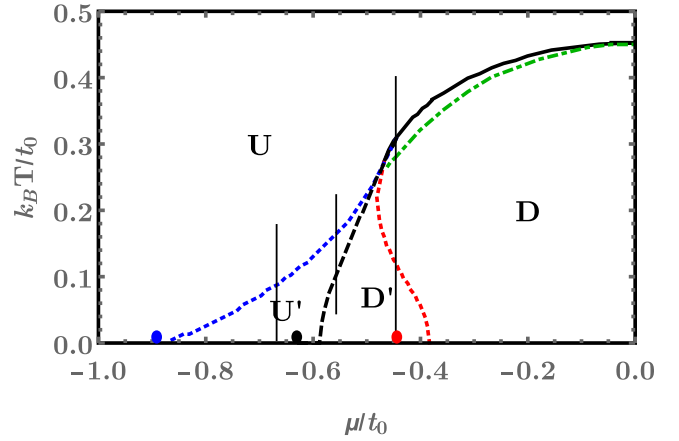


FIG. 9. Phase diagram (μ, T) of the SSH model in the mean-field approximation for an electron-phonon coupling $\lambda = 0.37$. The black solid and dashed lines show the phase boundary $T_P(\mu)$ between the dimerized phase (labeled D or D') and the uniform phase (labeled U or U'). The uniform configuration is metastable in the sector labeled D' while the dimerized state is metastable in the sector labeled U'. The solid line indicates the continuous phase transition between the sectors D and U while the dashed line indicates the first-order transition between the sectors D' and U' with metastable configurations. The dot-dashed line indicates the position of the first-order metal-insulator transition within the dimerized phase. Circles show the zero-temperature boundaries predicted by the weak-coupling analysis. Vertical lines indicate the values of μ and the temperature ranges considered in Figs. 10 to 12.

stable. In the smaller sectors D' and U' the other state is metastable. We denote $T_D(\mu)$ [or $\mu_D(T)$] the boundary line between the sectors U and U', where the metastable dimerized configurations vanish. Similarly, $T_U(\mu)$ [or $\mu_U(T)$] denotes the boundary line between the sectors D and D', where the metastable uniform configuration vanishes. The dimerized and uniform phases coexist only on the boundary between the sectors D' and U'. The coexistence terminates at a critical point (T_c, μ_c) . We could not estimate this point analytically but from the solution of the self-consistency equation (39) we obtain the position $k_B T_c \approx 0.25t_0$ and $\mu_c \approx -0.48t_0$ for $\lambda = 0.37$.

The transition between the sectors D and U is continuous while it is first-order between the sectors with metastable configurations D' and U'. Note that the boundary of the sector D at finite T and μ is given by the solutions of the self-consistency equation (40) while the boundary of the sector U is determined by the solution of the self-consistency equation (39) with the highest temperature for a given chemical potential. The boundary between the sectors D' and U' is given by the solutions of (39) with the same potential (15) as the uniform configuration $\delta = 0$.

Figure 9 reveals that the sector boundaries at low temperature [$\mu_D(T \rightarrow 0) \approx -0.87t_0$, $\mu_P(T \rightarrow 0) \approx -0.586t_0$, and $\mu_U(T \rightarrow 0) \approx -0.385t_0$] are close to the ground-state results of Sec. IV A [$\mu_D(T = 0) = -\Delta_0 \approx -0.891t_0$, $\mu_P(T = 0) = -\Delta_0/\sqrt{2} \approx -0.630t_0$, and $\mu_U(T = 0) = -\Delta_0/2 \approx -0.446t_0$], although deviations are clearly visible for the electron-phonon coupling $\lambda = 0.37$ used here. For smaller electron-phonon couplings, such as

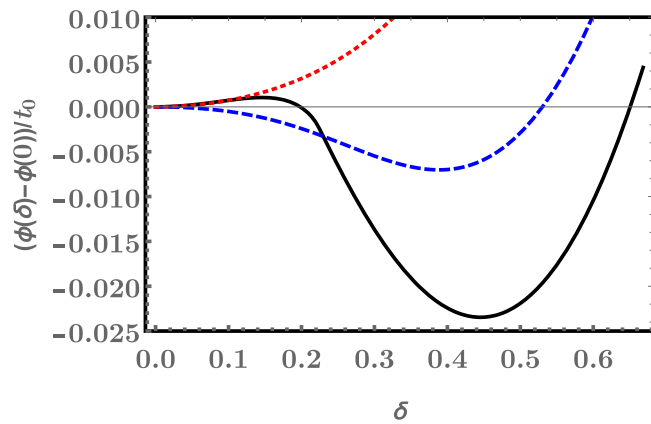


FIG. 10. Grand-canonical potential (15) as a function of the order parameter $\delta \geq 0$ for $\lambda = 0.37$, $\mu = -0.5\Delta_0 \approx -0.446t_0$, and several temperatures $k_B T = 0.005\Delta_0 \approx 0.00446t_0$ (black solid line), $k_B T = 0.225\Delta_0 \approx 0.201t_0$ (blue dashed line), and $k_B T = 0.45\Delta_0 \approx 0.401t_0$ (red dotted line).

$\lambda = 0.18$, the phase diagram determined numerically using Eqs. (39) and (40) agree quantitatively with the ground-state boundaries given in Sec. IV A.

In the phase diagram in Fig. 9 we also see that the system moves rapidly through the four sectors if one changes the chemical potential at fixed but low temperature. In particular, the system undergoes a first-order transition at the critical value $\mu_P(T)$. This could explain the sensitivity of the In/Si(111) system to the chemical doping of the substrate [13,24–26], which corresponds to changing the chemical potential in our model.

To understand this phase diagram better we discuss the evolution of the system when temperature is raised at a fixed chemical potential in more details. There are three unusual scenarios that can happen depending on the value of the chemical potential: $\mu_U(T=0) > \mu > \mu_c$, $\mu_c > \mu > \mu_P(T=0)$, and $\mu_P(T=0) > \mu > \mu_D(T=0)$. The variations of the grand-canonical potential are illustrated in Figs. 10–12 for

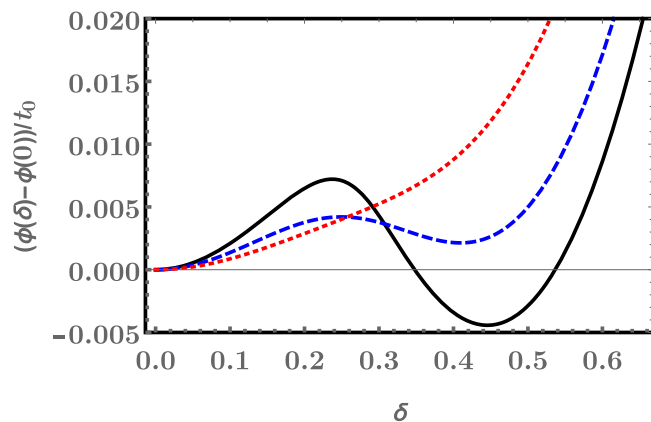


FIG. 11. Grand-canonical potential (15) as a function of the order parameter $\delta \geq 0$ for $\lambda = 0.37$, $\mu = -0.625\Delta_0 \approx -0.557t_0$, and several temperatures $k_B T = 0.05\Delta_0 \approx 0.0446t_0$ (black solid line), $k_B T = 0.15\Delta_0 \approx 0.134t_0$ (blue dashed line), and $k_B T = 0.25\Delta_0 \approx 0.223t_0$ (red dotted line).

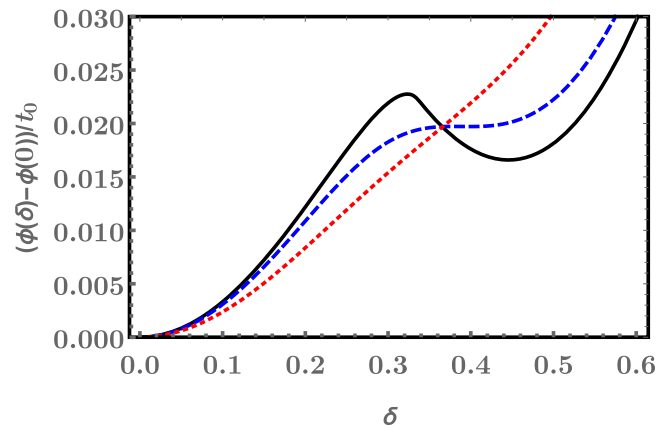


FIG. 12. Grand-canonical potential (15) as a function of the order parameter $\delta \geq 0$ for $\lambda = 0.37$, $\mu = -0.75\Delta_0 \approx -0.668t_0$, and several temperatures $k_B T = 0.005\Delta_0 \approx 0.00446t_0$ (black solid line), $k_B T = 0.1\Delta_0 \approx 0.0891t_0$ (blue dashed line), and $k_B T = 0.2\Delta_0 \approx 0.178t_0$ (red dotted line).

these three cases. For comparison, the variation of the free energy with temperature can be seen in Fig. 3 for the usual continuous Peierls transition at a fixed band filling. This scenario remains qualitatively valid as long as the uniform configuration is unstable at low temperature, explicitly for $\mu > \mu_U(T=0)$ with $\mu_U(T=0) \approx -0.385t_0$ for $\lambda = 0.37$ in the phase diagram in Fig. 9.

We consider first $\mu = -0.5\Delta_0 \approx -0.446t_0$, which lies between $\mu_U(T=0) \approx -0.385t_0$ and $\mu_c \approx -0.48t_0$. We see in the phase diagram in Fig. 9 that for this value of μ the system is dimerized with a metastable uniform phase at low temperature but moves from the sector D' to the sector D with increasing T because the metastable uniform configuration vanishes for temperatures higher than $k_B T_U(\mu) \approx 0.11t_0$. Then the system undergoes a continuous transition to the uniform phase U at a critical temperature $k_B T_P(\mu) \approx 0.307t_0$. The grand-canonical potential (15) shown in Fig. 10 changes accordingly, from a function with absolute minima for finite δ and a local minimum at $\delta = 0$ for a temperature lower than $T_U(\mu)$, to the usual double-well shape for a temperature between $T_U(\mu)$ and $T_P(\mu)$, and finally to a single-well shape for a temperature higher than $T_P(\mu)$.

Second, we examine the case of a chemical potential $\mu = -0.625\Delta_0 \approx -0.557t_0$, which lies between $\mu_c \approx -0.48t_0$ and $\mu_P(T=0) \approx -0.586t_0$. We see in the phase diagram in Fig. 9 that the system is again dimerized with a metastable uniform phase at low temperature for this value of μ . However, it now undergoes a first-order transition from the sector D' to the sector U' at the critical temperature $k_B T_P(\mu) \approx 0.102t_0$. As the temperature increases further the system moves into the sector U because the metastable dimerized configurations vanish above $k_B T_D(\mu) \approx 0.165t_0$. The grand-canonical potential (15) in Fig. 11 changes accordingly, from a function with absolute minima for finite δ and a local minimum at $\delta = 0$ for a temperature lower than $T_P(\mu)$ to a function with an absolute minimum at $\delta = 0$ and local minima for finite δ between $T_P(\mu)$ and $T_D(\mu)$, and finally exhibits the usual single-well shape for a temperature higher than $T_D(\mu)$.

Third, we discuss the case of $\mu = -0.75\Delta_0 \approx -0.668t_0$, which lies between $\mu_P(T=0) \approx -0.586t_0$ and $\mu_D(T=0) \approx -0.87t_0$. In that case the system remains within the uniform phase for all temperatures but moves from the sector U' to the sector U as the temperature is raised because the metastable dimerized state vanishes for temperatures higher than $k_B T_D(\mu) \approx 0.087t_0$. Accordingly, Fig. 12 shows that the grand-canonical potential (15) changes from a function with an absolute minimum at $\delta = 0$ and local minima at finite δ for a temperature below $T_D(\mu)$ to the usual single-well shape for high temperatures.

The above discussion completely describes the structural transition, which is uniquely determined by the order parameter through Eq. (6). The order parameter also determines the size of the electronic gap E_g that is open by the Peierls lattice distortion through Eq. (13). The vanishing of $\delta(T, \mu)$ implies the closing of this gap and thus in a Peierls transition at fixed band filling the metal-insulator transition occurs simultaneously to the structural transition and is also continuous. At a fixed chemical potential, however, the metal-insulator transition occurs when the chemical potential reaches the upper edge of the valence band, i.e., when $\mu = E_g/2 = -\Delta(T, \mu)$. Thus this transition can take place at a lower temperature than the structural transition and in this case it is first order, as the gap jumps from 0 to E_g at this point. We have found that this scenario occurs in the sector D of the dimerized phase for all chemical potentials $0 > \mu > \mu_c$. The critical temperature for the metal-insulator transition is shown in Fig. 9 and is in fact slightly lower than $T_P(\mu)$ for a given μ . As the structural transition is first order for $\mu < \mu_c$, we conclude that the metal-insulator transition is first order for all $0 > \mu > \mu_P(T=0)$ in the dimerized SSH model in the mean-field approximation.

C. First-order Peierls transition

With a view to understanding the first-order transition in In/Si(111), the most interesting part of the phase diagram is the region with a chemical potential between μ_c and $\mu_P(T=0)$. As discussed above, this leads to a first-order transition from the dimerized insulating phase at low temperature to a metallic uniform phase at high temperature with a metastable uniform configuration below the critical temperature. This agrees with the experimental observations for In/Si(111) [9–16]. Therefore, we examine the physical properties of the SSH model in that regime using the parameter $\lambda = 0.37$ and $\mu = -0.625\Delta_0 \approx -0.557t_0$ corresponding to the second case discussed above in the previous section.

As discussed in Sec. II the order parameter $\delta(T, \mu) = \Delta(T, \mu)/(2t_0)$ determines both the lattice deformation u through Eq. (6) and the electronic gap E_g through Eq. (13). Figure 13 shows the order parameter δ as a function of temperature through the first-order transition. We see that δ diminishes first progressively as the temperature rises from $T = 0$ to $k_B T_P(\mu) \approx 0.165t_0$, above which the dimerized state becomes unstable and δ drops to zero. However, the dimerized state is thermodynamically stable only up to the lower critical temperature $k_B T_P(\mu) \approx 0.102t_0$ and thus the first-order structural and metal-insulator transition takes place already at this temperature. This is in strong contrast to the continuous

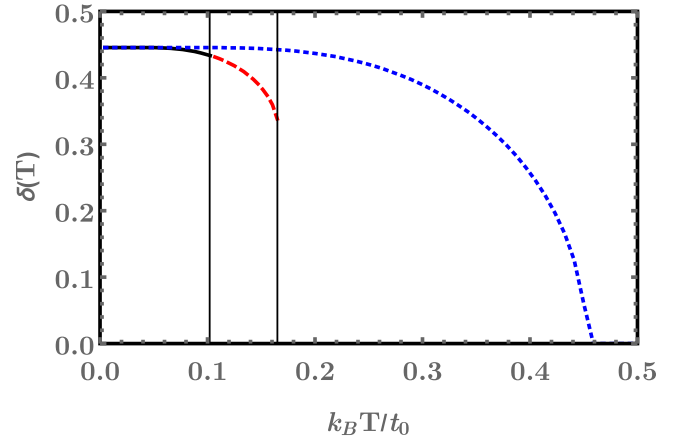


FIG. 13. Order parameter δ as a function of temperature for $\lambda = 0.37$. The vertical lines indicate the critical temperature $k_B T_P(\mu) \approx 0.102t_0$ and $k_B T_D(\mu) \approx 0.165t_0$ for $\mu = -0.625\Delta_0 \approx -0.557t_0$. The solid black and red dashed lines show δ for the thermodynamically stable dimerized phase [$T < T_P(\mu)$] and the metastable dimerized state [$T_P(\mu) < T < T_D(\mu)$] at this value of μ , respectively. The blue dotted line shows $\delta(T)$ at half-filling ($\mu = 0$).

Peierls transition at half-filling ($\mu = 0$), which is also shown in Fig. 13.

Another interesting physical quantity is the frequency of the Raman-active amplitude oscillations of the order parameter [2,20–22], which can be measured experimentally for In/Si(111) [14,15]. Figure 14 shows the renormalized phonon frequency $\Omega(T)/\omega_0$ calculated from Eq. (26) as a function of temperature through the first-order transition. We see that the frequency of the thermodynamically stable state diminishes progressively as the temperature rises from $T = 0$ to $k_B T_P(\mu) \approx 0.102t_0$. At this critical temperature the phonon frequency jumps to a lower value and then changes again

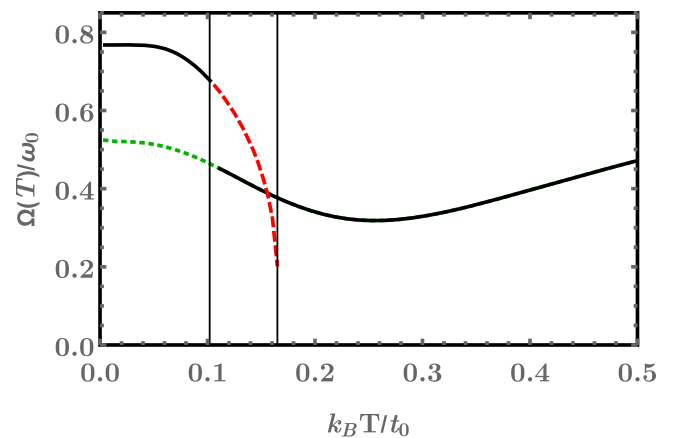


FIG. 14. Renormalized phonon frequency Ω/ω_0 [Eq. (26)] as a function of temperature for $\lambda = 0.37$ and $\mu = -0.625\Delta_0 \approx -0.557t_0$. The vertical lines indicate the critical temperature $k_B T_P(\mu) \approx 0.102t_0$ and $k_B T_D(\mu) \approx 0.165t_0$. The solid black line shows Ω in the thermodynamically stable phases with a jump at $T = T_P(\mu)$. The green dotted and red dashed lines show the frequency for the metastable uniform configuration below $T_P(\mu)$ and the metastable dimerized configurations for $T_P(\mu) < T < T_D(\mu)$, respectively.

smoothly as the temperature increases further. [For μ close to μ_c the frequency can also jump up at $T_p(\mu)$]. This jump of $\Omega(T)$ corresponds to the abrupt transition from oscillations around the dimerized configurations to oscillations around the uniform configuration. This variation of the phonon frequency with the temperature is in strong contrast to the complete phonon softening found in a continuous Peierls transition at fixed band filling and shown in Fig. 5.

In Fig. 14 we also show the phonon frequencies for oscillations around the metastable configurations. They prolong smoothly the curves $\Omega(T)/\omega_0$ obtained for the stable configurations. Note that amplitude oscillations around the dimerized configurations have the wave number $Q = 2k_F = \pi/a$ but they appear at $Q = 0$ in experiments below the critical temperature $T_p(\mu)$ because of the folding of the Brillouin zone due to the lattice dimerization. Oscillations around the uniform configuration always correspond to $Q = 0$.

V. CONCLUSION

We have investigated the grand-canonical Peierls transition in the SSH model in the mean-field approximation. We have found that the phase diagram is much richer than for the Peierls theory at fixed band filling. This could explain the sensitivity of the transition in In/Si(111) to chemical doping of the substrate [13,24–26]. Notably, we have found a first-order Peierls transition from the insulating dimerized phase to the metallic uniform phase when temperature is raised at a fixed chemical potential. Moreover, the uniform phase remains metastable below the critical temperature. These findings agree with experimental evidence and first-principles simulations for In/Si(111) [9–16]. Therefore, we think that this grand-canonical Peierls theory is the appropriate basis for describing the quasi-one-dimensional physics realized in the In/Si(111) system.

The SSH model is a minimal model for a commensurate Peierls transition and we have investigated its phase diagram using a basic mean-field approach. Thus we briefly discuss some effects that we have neglected and possible extensions of the present work.

Our approach neglects spatial fluctuations of the lattice distortion u_j . Away from half-filling ($\mu \neq 0$) the lattice is probably unstable with respect to incommensurate Peierls distortions, such as

$$u_j = \tilde{u} \cos(Qja + \phi), \quad (41)$$

with appropriate amplitude \tilde{u} and wave number Q as well as an arbitrary phase ϕ . (The wave number would be $Q = 2k_F$ in the Peierls theory at fixed band filling [2]). However, these incommensurate distortions have a much lower critical temperature than the dimerization. Moreover, the coupling between atomic wires and the periodic substrate lattice should render them even less energetically stable. Thus we do not expect them to play any significant role as long as $\mu > -\Delta_0$, but they could become relevant in the sector U of the uniform phase at very low temperature.

A more interesting effect of spatial fluctuations of the order parameter is that the dimerized phase could be unstable with respect to the formation of domain walls between both dimerized configurations (so-called solitons). The

theoretical modeling of solitons is a key feature of the SSH model [3,4,17,18] and the existence and properties of solitons in the In/Si(111) system are still debated [27–33]. Therefore, it would be interesting to extend the grand-canonical Peierls theory to describe solitons.

Besides spatial fluctuations, thermal and quantum lattice fluctuations are important in low-dimensional systems [2,4,34–36]. It is well known that a spontaneous symmetry breaking such as the dimerization cannot occur at finite temperature in a one-dimensional systems with finite range interactions because of thermal fluctuations. However, it is also well established that true finite-temperature phase transitions may take place in quasi-one-dimensional systems made of a higher dimensional array of (weakly) coupled chains because the fluctuations are suppressed by the ordering perpendicular to the chains [19,34,35]. In atomic wires on substrates, both this coupling between wires and the coupling of the wires to the substrate suppress fluctuations and thus will allow for a Peierls transition at finite temperature. Nevertheless, it will be necessary to extend the present work to include interwire coupling combined with thermal and quantum fluctuations to study the phase transition and the system properties in the critical regime more accurately. Their effects can be studied in SSH-like models using sophisticated numerical methods such as quantum Monte Carlo simulations [37–39]. However, we think that our results for the first-order transition and the metastable states away from the critical point (T_c, μ_c) will remain qualitatively valid when they are taken into account. The main combined effects of interwire coupling and fluctuations will be to reduce the various temperatures calculated within the mean-field semiclassical approach, as it was found for the Peierls theory at fixed band filling [2,22,35,36].

Electronic correlation effects are also neglected in the SSH model as they do not play a determinant role in the Peierls theory. Typically, one assumes that the Coulomb repulsion between electrons only renormalizes the model parameters such as the electron-phonon coupling [3]. However, it is known that they can be important for a correct description of important aspects of the Peierls physics [4,40,41], such as the insulating dimerized phase with domain walls away from half-filling (soliton lattice) [42,43] or the possible Luttinger liquid properties of the metallic phase just above the critical temperature [6]. Therefore, it could be interesting to study the grand-canonical Peierls transition in generalizations of the SSH model including the electron-electron interaction explicitly.

In summary, our study of the Peierls transition in the grand-canonical ensemble reveals a rich phase diagram, which includes a first-order Peierls transition between regions with metastable uniform and dimerized states as well as a region with a first-order metal-insulator transition at a lower temperature than the continuous structural transition. Various aspects neglected in the present work should be investigated next but we are confident that our main findings will remain relevant.

ACKNOWLEDGMENTS

This work was done as part of the Research Unit *Metallic nanowires on the atomic scale: Electronic and vibrational coupling in real world systems* (FOR1700) of the German

Research Foundation (DFG) and was supported by Grant No. JE 261/1-2.

APPENDIX A: HOPPING TERM

The SSH linear approximation for the hopping term (4) is not consistent with the harmonic approximation for the lattice elastic energy (2) because second-order contributions of the lattice displacements u_j to the electronic energy are thus neglected. As an example, consider a (more accurate) exponential dependence of the hopping terms on the distance variation between sites [44,45]

$$t(u_{j+1} - u_j) = t_0 \exp[-\alpha(u_{j+1} - u_j)/t_0]. \quad (\text{A1})$$

Expanding up to second order yields

$$t(u_{j+1} - u_j) = t_0 - \alpha(u_{j+1} - u_j) + \frac{\alpha^2}{2t_0}(u_{j+1} - u_j)^2. \quad (\text{A2})$$

This agrees with the SSH hopping term (4) up to first order in the displacements u_j but the second order term is completely neglected in the SSH model. Using the second-order expansion (A2) and the dimerized configuration (5), we recover the electronic dispersion (12) but with

$$\tilde{t}_0 = t_0 \left(1 + \frac{1}{2}\delta^2\right) \quad (\text{A3})$$

substituted for t_0 . An analysis similar to the one carried out in Sec. III leads to similar results, in particular the zero-temperature order parameter is given by

$$\tilde{\delta}_0 = \frac{\tilde{\Delta}_0}{2t_0} = 4 \exp\left(-\frac{1}{2\lambda}\right) \quad (\text{A4})$$

in the weak-coupling limit. This differs by a constant factor e^{-1} from the SSH result (24). Therefore, disregarding the second-order term in (A2) leads to a quantitatively incorrect result.

This factor does not play any role in the qualitative investigation of the SSH model properties, however, because there is a one-to-one relation between the order parameter and the only model parameter λ . As the renormalization of the bare hopping term (A3) is otherwise negligible in the weak-coupling limit, this allows us to express all observables

directly as a function of $\tilde{\delta}_0$ rather than λ and to verify that the (weak-coupling) model properties depend on δ_0 [for the hopping term (4)] exactly as on $\tilde{\delta}_0$ [for the hopping term (A2)]. Therefore, the different prefactors in Eqs. (24) and (A4) [as well as (30)] must only be taken into account when comparing to numerical simulation of the SSH model [14], first-principles simulations, or experimental results.

APPENDIX B: ZERO-TEMPERATURE SELF-CONSISTENCY EQUATION AWAY FROM HALF-FILLING

From the general self-consistency equation (39) one obtains for $T \rightarrow 0$

$$\frac{1 - \delta^2}{2\lambda} 2t_0 = \int_{\Lambda} d\varepsilon \sqrt{\frac{4t_0^2 - \varepsilon^2}{\varepsilon^2 - \Delta^2}}, \quad (\text{B1})$$

where Λ is the largest of $|\Delta|$ and $|\mu|$. Assuming again a linear electronic dispersion with a cutoff $2t_0$ for $|\varepsilon| \gg |\Delta|$ and $|\delta| \ll 1$, we obtain the same self-consistency equation for $\Lambda = |\Delta|$ as for half-filling and thus the same result (30) for the solution δ'_0 . Thus there are two (possibly local) minima at $\pm\delta'_0$ for $0 \geq \mu \geq -\Delta'_0 = 2\delta'_0 t_0$ and no extrema with $|\Delta| > |\mu| > \Delta'_0$. For $\Lambda = |\mu|$ the self-consistency equation becomes

$$\ln\left(\frac{\Delta'_0}{|\Delta|}\right) = \text{acosh}\left(\frac{|\mu|}{|\Delta|}\right) \geq 0. \quad (\text{B2})$$

Obviously there is no solution with $|\mu| > |\Delta| > \Delta'_0$. Consequently, there are no extrema with $\delta \neq 0$ for any $\mu < -\Delta'_0$. We see that the above equation possesses solutions $\pm\Delta' \neq 0$ starting from $\Delta' = 0$ for $\mu = -\Delta'_0/2$ and increasing continuously up to $\Delta' = \Delta'_0$ for $\mu = -\Delta'_0$. One can check numerically that these solutions of the self-consistency equation correspond to local maxima. Thus this analysis confirms the existence of simultaneous minima for the uniform and dimerized configurations when $-\Delta'_0/2 > \mu > -\Delta'_0$ in agreement with the discussion of Eq. (34) in Sec IV A. Moreover, the absence of any solution of the self-consistency equation for $\mu < -\Delta'_0$ shows that the dimerized state is unstable in this regime.

-
- [1] R. E. Peierls, *Quantum Theory of Solids* (Oxford University Press, London, 1956).
- [2] G. Grüner, *Density Waves in Solids* (Perseus, Cambridge, 2000).
- [3] A. J. Heeger, S. Kivelson, J. R. Schrieffer, and W.-P. Su, Solitons in conducting polymers, *Rev. Mod. Phys.* **60**, 781 (1988).
- [4] D. Baeriswyl, D. K. Campbell, and S. Mazumdar, An overview of the theory of π -conjugated polymers, *Conjugated Conducting Polymers*, edited by H. Kiess (Springer, Berlin, 1992), Chap. 2.
- [5] J. Sólyom, *Fundamentals of the Physics of Solids, Volume 3 - Normal, Broken-Symmetry, and Correlated Systems* (Springer, Berlin, 2010).
- [6] N. Oncel, Atomic chains on surfaces, *J. Phys.: Condens. Matter* **20**, 393001 (2008).
- [7] P. C. Snijders and H. H. Weitering, Colloquium: Electronic instabilities in self-assembled atom wires, *Rev. Mod. Phys.* **82**, 307 (2010).
- [8] H. W. Yeom, S. Takeda, E. Rotenberg, I. Matsuda, K. Horikoshi, J. Schaefer, C. M. Lee, S. D. Kevan, T. Ohta, T. Nagao, and S. Hasegawa, Instability and Charge Density Wave of Metallic Quantum Chains on a Silicon Surface, *Phys. Rev. Lett.* **82**, 4898 (1999).
- [9] S. Hatta, Y. Ohtsubo, T. Aruga, S. Miyamoto, H. Okuyama, H. Tajiri, and O. Sakata, Dynamical fluctuations in nanowires on Si(111), *Phys. Rev. B* **84**, 245321 (2011).
- [10] S. Wall, B. Krenzer, S. Wippermann, S. Sanna, F. Klasing, A. Hanisch-Blicharski, M. Kammler, W. G. Schmidt, and M. Horn-von Hoegen, Atomistic Picture of Charge Density Wave Formation at Surfaces, *Phys. Rev. Lett.* **109**, 186101 (2012).

- [11] W. G. Schmidt, S. Wippermann, S. Sanna, M. Babilon, N. J. Vollmers, and U. Gerstmann, In-Si(111) (4×1)/(8×2) nanowires: Electron transport, entropy, and metal-insulator transition, *Phys. Status Solidi B* **249**, 343 (2012).
- [12] F. Klasing, T. Frigge, B. Hafke, B. Krenzer, S. Wall, A. Hanisch-Blicharski, and M. Horn-von Hoegen, Hysteresis proves that the In/Si(111) (8×2) to (4×1) phase transition is first-order, *Phys. Rev. B* **89**, 121107(R) (2014).
- [13] H. Zhang, F. Ming, H.-J. Kim, H. Zhu, Q. Zhang, H. H. Weitering, X. Xiao, C. Zeng, J.-H. Cho, and Z. Zhang, Stabilization and Manipulation of Electronically Phase-Separated Ground States in Defective Indium Atom Wires on Silicon, *Phys. Rev. Lett.* **113**, 196802 (2014).
- [14] E. Jeckelmann, S. Sanna, W. G. Schmidt, E. Speiser, and N. Esser, Grand canonical Peierls transition in In/Si(111), *Phys. Rev. B* **93**, 241407(R) (2016).
- [15] E. Speiser, N. Esser, S. Wippermann, and W. G. Schmidt, Surface vibrational Raman modes of In/Si(111)(4×1) and (8×2) nanowires, *Phys. Rev. B* **94**, 075417 (2016).
- [16] S. Hatta, T. Noma, H. Okuyama, and T. Aruga, Electrical conduction and metal-insulator transition of indium nanowires on Si(111), *Phys. Rev. B* **95**, 195409 (2017).
- [17] W. P. Su, J. R. Schrieffer, and A. J. Heeger, Solitons in Polyacetylene, *Phys. Rev. Lett.* **42**, 1698 (1979).
- [18] W. P. Su, J. R. Schrieffer, and A. J. Heeger, Soliton excitations in polyacetylene, *Phys. Rev. B* **22**, 2099 (1980).
- [19] J. Sólyom, *Fundamentals of the Physics of Solids, Volume 2 - Electronic Properties* (Springer, Berlin, 2009).
- [20] H. J. Schulz, Lattice dynamics and electrical properties of commensurate one-dimensional charge-density-wave systems, *Phys. Rev. B* **18**, 5756 (1978).
- [21] B. Horowitz, H. Gutfreund, and M. Weger, Infrared and Raman activities of organic linear conductors, *Phys. Rev. B* **17**, 2796 (1978).
- [22] E. Tutiš and S. Barišić, Dynamic structure factor of a one-dimensional Peierls system, *Phys. Rev. B* **43**, 8431 (1991).
- [23] B. Horowitz, Infrared activity of Peierls systems and application to polyacetylene, *Solid State Commun.* **41**, 729 (1982).
- [24] H. Shim, S.-Y. Yu, W. Lee, J.-Y. Koo, and G. Lee, Control of phase transition in quasi-one-dimensional atomic wires by electron doping, *Appl. Phys. Lett.* **94**, 231901 (2009).
- [25] H. Morikawa, C. C. Hwang, and H. W. Yeom, Controlled electron doping into metallic atomic wires: Si(111) 4×1 -In, *Phys. Rev. B* **81**, 075401 (2010).
- [26] W. G. Schmidt, M. Babilon, C. Thierfelder, S. Sanna, and S. Wippermann, Influence of Na adsorption on the quantum conductance and metal-insulator transition of the In-Si(111)(4×1)-(8 \times 2) nanowire array, *Phys. Rev. B* **84**, 115416 (2011).
- [27] H. Morikawa, I. Matsuda, and S. Hasegawa, Direct observation of soliton dynamics in charge-density waves on a quasi-one-dimensional metallic surface, *Phys. Rev. B* **70**, 085412 (2004).
- [28] H. Zhang, J.-H. Choi, Y. Xu, X. Wang, X. Zhai, B. Wang, C. Zeng, J.-H. Cho, Z. Zhang, and J. G. Hou, Atomic Structure, Energetics, and Dynamics of Topological Solitons in Indium Chains on Si(111) Surfaces, *Phys. Rev. Lett.* **106**, 026801 (2011).
- [29] H. W. Yeom and T.-H. Kim, Comment on “Atomic Structure, Energetics, and Dynamics of Topological Solitons in Indium Chains on Si(111) Surfaces”, *Phys. Rev. Lett.* **107**, 019701 (2011).
- [30] H. Zhang, J.-H. Choi, Y. Xu, X. Wang, X. Zhai, B. Wang, C. Zeng, J.-H. Cho, Z. Zhang, and J. G. Hou, Reply to a Comment on “Atomic Structure, Energetics, and Dynamics of Topological Solitons in Indium Chains on Si(111) Surfaces”, *Phys. Rev. Lett.* **107**, 019702 (2011).
- [31] T.-H. Kim and H. W. Yeom, Topological Solitons versus Non-solitonic Phase Defects in a Quasi-One-Dimensional Charge-Density Wave, *Phys. Rev. Lett.* **109**, 246802 (2012).
- [32] S. Cheon, T.-H. Kim, S.-H. Lee, and H. W. Yeom, Chiral solitons in a coupled double Peierls chain, *Science* **350**, 182 (2015).
- [33] G. Lee, H. Shim, J.-M. Hyun, and H. Kim, Intertwined Solitons and Impurities in a Quasi-One-Dimensional Charge-Density-Wave System: In/Si(111), *Phys. Rev. Lett.* **122**, 016102 (2019).
- [34] D. Baeriswyl and L. Degiorgi, *Strong Interactions in Low Dimensions* (Kluwer Academic, Dordrecht, 2004).
- [35] B. Horowitz, H. Gutfreund, and M. Weger, Interchain coupling and the Peierls transition in linear-chain systems, *Phys. Rev. B* **12**, 3174 (1975).
- [36] P. A. Lee, T. M. Rice, and P. W. Anderson, Fluctuation Effects at a Peierls Transition, *Phys. Rev. Lett.* **31**, 462 (1973).
- [37] M. Weber, F. F. Assaad, and M. Hohenadler, Thermodynamic and spectral properties of adiabatic Peierls chains, *Phys. Rev. B* **94**, 155150 (2016).
- [38] M. Hohenadler and H. Fehske, Density waves in strongly correlated quantum chains, *Eur. Phys. J. B* **91**, 204 (2018).
- [39] M. Weber, F. F. Assaad, and M. Hohenadler, Thermal and quantum lattice fluctuations in Peierls chains, *Phys. Rev. B* **98**, 235117 (2018).
- [40] W. Barford, *Electronic and Optical Properties of Conjugated Polymers*, International Series of Monographs on Physics (Oxford University Press, Oxford, 2013).
- [41] M. Timár, G. Barcza, F. Gebhard, and O. Legeza, Optical phonons for Peierls chains with long-range Coulomb interactions, *Phys. Rev. B* **95**, 085150 (2017).
- [42] E. Jeckelmann and D. Baeriswyl, The metal-insulator transition in polyacetylene: Variational study of the Peierls-Hubbard model, *Synth. Met.* **65**, 211 (1994).
- [43] E. Jeckelmann, Mott-Peierls transition in the extended Peierls-Hubbard model, *Phys. Rev. B* **57**, 11838 (1998).
- [44] H. C. Longuet-Higgins and L. Salem, The alternation of bond lengths in long conjugated chain molecules, *Proc. R. Soc. London Ser. A* **251**, 172 (1959).
- [45] L. Salem and H. C. Longuet-Higgins, The alternation of bond lengths in long conjugated molecules. II. The polyacenes, *Proc. R. Soc. London Ser. A* **255**, 435 (1960).